

Design and Verification of Free Space Optical Communication Relay Between Ground and Tethered Ball

YU Siyuan, LI Bo*, CAO Kairui, HAO Guanglu, DU Hairui

National Key Laboratory of Tunable Laser Technology, Harbin Institute of Technology, Harbin 150001, P.R.China

(Received 2 April 2022; revised 1 November 2022; accepted 3 January 2023)

Abstract: There are currently some deficiencies with microwave mobile relay networks, such as short relay distance, sluggish data transfer rate, high power consumption, and limited operating frequency. This paper builds a relay system using laser communication technology to complete real-time forwarding of infrared high-definition data within a distance of more than 20 km from the tethered aerostat and the ground base station. This experiment's success serves as a technical reference for the use of laser communication technology as an airborne communication relay station. A scanning acquisition scheme and attitude stability compensation scheme based on probability statistics are proposed to address the uncertain initial pointing angle and the external conditions of the rapid change of platform attitude. To avoid the complex integral calculation, this paper proposes a method based on the fourth-order Runge-Kutta to improve the algorithm's accuracy while ensuring the function's realization. The feedforward speed is introduced into the speed loop of the closed-loop tracking system based on the spatial position of the target and the change in its own attitude, which effectively improves the system's tracking stability. We plan to conduct experiments on relaying laser links in air-to-air networks in the future.

Key words: space optical communication; laser link; pointing, acquisition and tracking

CLC number: TN929.13

Document code: A

Article ID: 1005-1120(2023)01-0060-11

0 Introduction

With the widespread use of big data and cloud computing in recent years, the requirements for data transmission rate and real-time performance have greatly improved. 5G (The fifth generation) communication technology is capable of meeting its requirements and has been widely used in many countries. However, due to the high cost of base station construction and the difficulty of remote transmission^[1-7], it is unable to provide comprehensive coverage. We can effectively solve these problems by deploying unmanned aerial vehicles, tethered balls, and other airbase platforms^[8-10].

To meet the needs of the modern age, the data transmission rate of a relay link should be several orders of magnitude higher than that of a single

node^[11]. Free-space optical (FSO) communication has a high bandwidth, secure transmission, is anti-interference, and is not limited by frequency band licensing, among other benefits^[12-13]. As a result, selecting FSO as the communication network supplement technology on the airbase platform is a wise decision^[14-15]. Meanwhile, it has extensible features that can significantly increase communication link capacity simply by increasing the wavelength^[16].

Some research groups have completed many great experiments in free space laser communication on the airbase platform. Deutsches Zentrum für Luft und Raumfahrt (DLR) announced the Project AR-GOS project in 2008. This project formed a wireless communication network by connecting the Do-228 aeroplane and ground station which were all

*Corresponding author, E-mail address: 54libolibo@163.com.

How to cite this article: YU Siyuan, LI Bo, CAO Kairui, et al. Design and verification of free space optical communication relay between ground and tethered ball[J]. Transactions of Nanjing University of Aeronautics and Astronautics, 2023, 40(1): 60-70.

<http://dx.doi.org/10.16356/j.1005-1120.2023.01.006>

equipped with laser communication terminals (LCT). The communication distance was 10—85 km, and the communication rate is 155 Mbit/s. In 2011, the communication demonstration test was further realized, the distance was increased to 100 km, and the communication rate was increased to 1.25 Gbit/s^[17]. In 2015, an airborne optical communication demonstrator was developed by Hensoldt, which provided air-to-space unidirectional communication capabilities over approximately 40 000 km distance (Geo orbit) at a data rate of 1.8 Gbit/s at a wavelength of 1 064 nm with a laser power of approximately 15 W. The demonstrator was flown on an Airbus A310 aircraft^[18]. In 2019, A dynamic space laser communications test between airship and ship was carried out by Changchun University of Science and Technology^[19]. These experiments have guiding significance for the application of FSO technology on airbase platforms.

This paper proposes a laser communication relay system based on a tethered ball platform to address the demands of long-distance and high-capacity data transfer. A downsized design of the separation of the optical module and the electrical module is presented to facilitate system update and maintenance, and the system's composition and operating principle are introduced. The technique and pointing, acquisition and tracking (PAT) approach for creating the laser communication link of the tethered ball platform are described. For the uncertain pointing angle, a scanning optimization technique based on probability and statistics is provided, and the Runge-Kutta algorithm is employed to avoid complicated integral calculations and increase the calculation accuracy of discrete systems. Simultaneously, the spatial position, attitude, and platform vibration compensation effect data of the experiment's tethered ball are provided. Finally, the communication system's performance is validated by sending real-time infrared high-definition data images, which provides technical support and theoretical validation for the use of laser communication technology in long-distance information relay scenarios.

1 Laser Link and LCT System Design

The LCT was installed on the ground and the tethered aerostat platform in this experiment. Use the high-definition infrared camera on the aerostat to film the ground facilities, and then send the dynamic video data to the ground terminal via a high-speed laser link. Finally, the data is distributed to the user equipment by the ground terminal. Fig.1 shows an image of the experimental site's equipment.

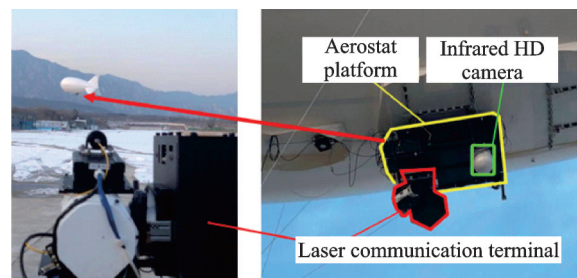


Fig.1 Laser link experiment

The laser link's communication distance is set to be 20 km, and the tethered ball's floating height is set to be 1 km. Through the network port, real-time data is transmitted between the infrared camera and the LCT. The communication rate of a single-wavelength laser is 2.5 Gbit/s. The wavelength division multiplexing technology can be used to improve the communication capacity of the link in subsequent engineering applications^[20].

The LCT uses an orthogonal axis, as shown in Fig.2(a). The optical component is installed on the elevation axis system, and the azimuth axis system is installed on the aerostat's platform pod to carry the entire terminal. The pointing range can cover the entire hemisphere, and the LCT's total mass and power consumption are less than 15 kg and 100 W, respectively.

Functions like power interface, modulation and demodulation, photoelectric signal conversion, motor and fast-steering mirror drive are provided by the electrical part. The LCT's current location and attitude are determined using data from the telemetry and remote control interface. The optical path and circuit are completely independent in this design. The optics and electronics modules can be updated

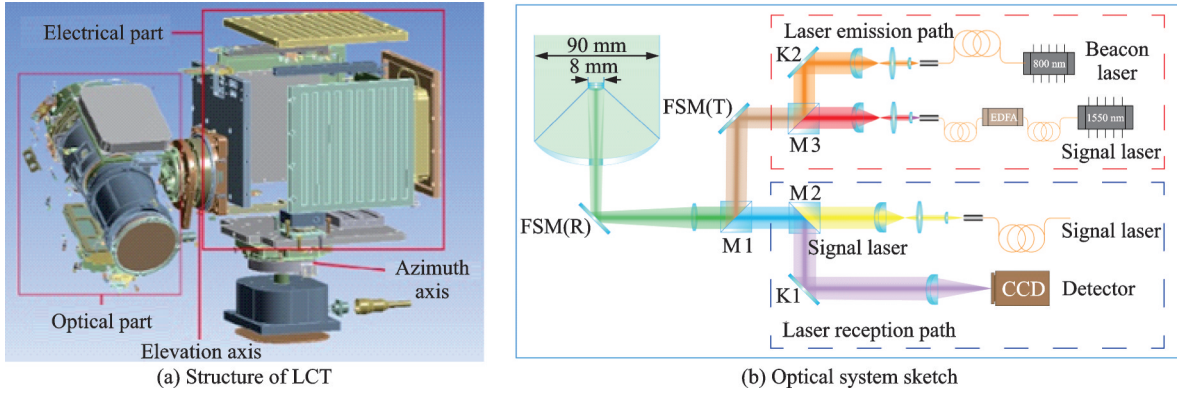


Fig.2 Design sketch

and maintained separately by retaining the interface definition, ensuring large-scale manufacturing and maintenance services.

Fig.2(b) depicts the optical system sketch. We chose the Cassegrain Telescope structure to provide a high magnification optical system^[21]. The primary mirror measures 90 mm in diameter, and the secondary mirror measures 8 mm in diameter. After the primary and secondary mirrors, the fast-steering mirror FSM(R) is used to precisely adjust the overall optical path to complete the spot tracking.

The transmitting optical path is coupled into the main beam via the beam splitters M1 and M3 to complete the sharing of the transmitting and receiving optical paths. FSM(T) can adjust the angle of the transmitting optical path to complete the function of aiming in advance. To facilitate tracking and communication, the beam splitter M2 separates the beams of the received signal and the beacon laser, and the beam splitting ratio is set to 99:1. The main parameters of LCT are listed in Table 1.

Table 1 Design parameters of LCT

Parameter	Value
Optical antenna aperture/mm	90
Operating wavelength/nm	1 535.04
Transmitted power/W	Signal: 0.1
	Beacon: 1
Range of pointing angle/(°)	Azimuth (Az): ± 180
	Elevation (El): 0—90
Detector field of view/mrad	2
Mass/kg	≤ 15
Power dissipation/W	≤ 100
Communication range/km	> 20
Communication rate/(Gbit·s ⁻¹)	2.5

2 System Control Scheme

2.1 Workflow

The workflow of air to ground laser relay link establishment is mainly divided into four stages, as shown in Fig.3.

Pointing mode is the first stage. It is a dynamic control process due to the relative angular movement between the two terminals. Ground stations and aerostat terminals can exchange GPS position data via separate radio links. The pointing angle can be calculated at any time by using the platform's attitude and position data. As a result, pointing accuracy will be affected by factors such as platform attitude, position, control precision, and platform vibration. The scanning range of the subsequent acquisition mode is determined by the pointing accuracy, which has a direct impact on capture performance. As a result, in order to achieve the best laser communication link performance, it is necessary to improve the accuracy of platform attitude measurement and position prediction as much as possible in the link system design.

The acquisition mode is made up of Stages 2 and 3. The primary task of Stage 2 is to complete the scanning action by controlling the rotating shaft so that the own detector can locate the beacon laser of the other. When one party detects the other party's beacon laser, Stage 3 of the task begins. A closed loop system composed of the detector and rotating shaft adjusts the position of the light spot to keep the laser spot within the working range of the fine control unit, and the acquisition mode is completed.

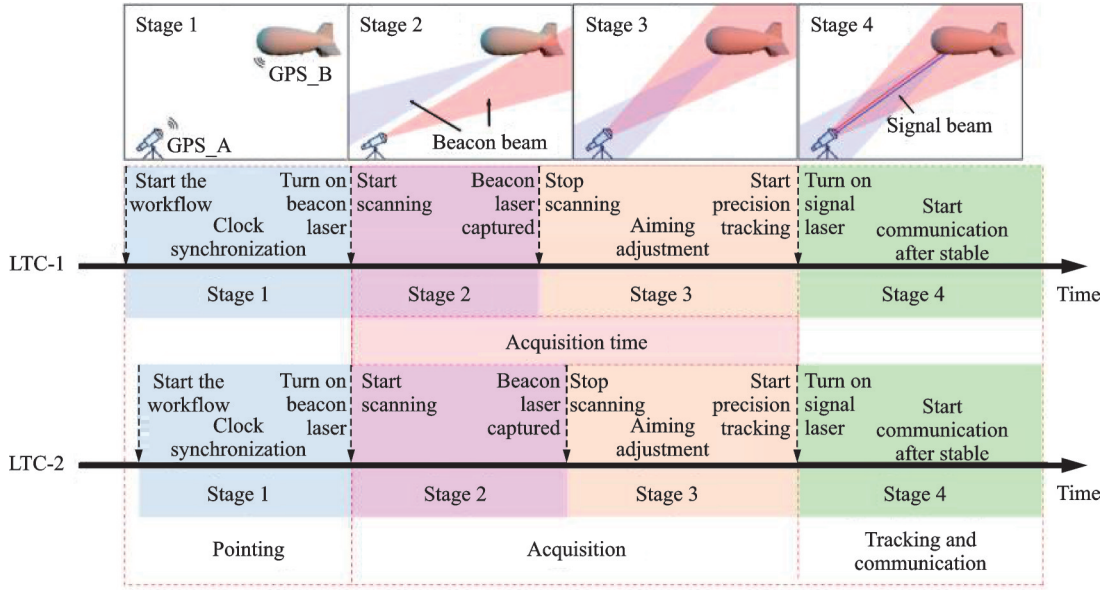


Fig.3 Workflow chart

Finally, the LCTs lock onto each other via the beacon laser, and the link enters tracking and communication mode. The terminal precise tracking system is activated, and the closed-loop control system sends the spot deviation to the precise aiming controller for immediate correction. The rotating shaft system and precise aiming controller are combined to form a new closed-loop system, whose function is to keep the FSM from exceeding the deflection range, allowing it to work continuously. When the tracking accuracy meets the communication requirements, it can initiate communication and transmit real-time high-definition image data. To reduce the bit error rate of laser communication, it is necessary to focus on compensating for the influence of platform vibration on tracking accuracy at this stage.

2.2 Pointing strategy

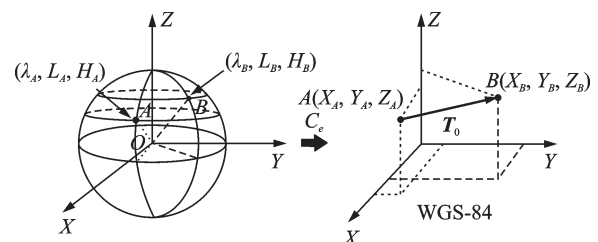
The ground and air terminals require precise initial pointing in order to quickly establish the laser relay network. The aiming vector problem has essentially gone through three stages. It used to be a straightforward plane rectangular coordinate formula. In the 1990s, two-dimensional coordinate transformations were handled using Vincenty's precision formula as well as the nautical Bowring's formula. We are currently using the algorithm for 3D space alignment.

This pointing angle can be calculated using the

carrier's position coordinates and attitude angle, which can be obtained via the platform's GPS/INS integrated navigation system. Since GPS, INS and terminal installations use different coordinate systems, the final aiming angle must be calculated using a series of coordinate transformations. A specific targeting strategy consists of the following components^[22].

(1) Using GPS, the local and target machine's laser terminal's latitude, longitude, and altitude information are obtained and converted into spatial position coordinates using the WGS-84 coordinate system, as shown in Fig.4. The spatial position pointing vector of T_0 can be computed by

$$T_0 = \begin{bmatrix} (N_B + H_B) \cos L_B \cos \lambda_B - \\ (N_A + H_A) \cos L_A \cos \lambda_A \\ (N_B + H_B) \cos L_B \sin \lambda_B - \\ (N_A + H_A) \cos L_A \sin \lambda_A \\ (N_B(1 - e^2) + H_B) \sin L_B - \\ (N_A(1 - e^2) + H_A) \sin L_A \end{bmatrix} \quad (1)$$

Fig.4 T_0 in WGS-84 coordinate system

where $N = a/\sqrt{1 - e^2 \sin^2 L}$, $a = 6\,378.137$ km; $e^2 = 0.006\,693\,437\,995$; λ , L and H represent the longitude, latitude and altitude of the spatial position, respectively. Both sides of the link are represented by the subscripts A and B .

(2) The position pointing vector obtained in the WGS-84 coordinate system is converted into the pointing vector T_1 in the ENU (east-north-up) coordinates, as shown in Fig. 5, which is commonly used in attitude calculation.

The matrix conversion C_e^g from WGS-84 to ENU coordinates system is shown as

$$C_e^g = \begin{pmatrix} -\sin \lambda_A & \cos \lambda_A & 0 \\ -\sin L_A \cos \lambda_A & -\sin L_A \sin \lambda_A & \cos L_A \\ \cos L_A \cos \lambda_A & \cos L_A \sin \lambda_A & \sin L_A \end{pmatrix} \quad (2)$$

(3) After obtaining the pointing vector T_1 in

$$C_T(\gamma, \psi, \theta) = \begin{pmatrix} \cos \psi \cos \theta & -\cos \theta \sin \psi & \sin \psi \\ \cos \theta \sin \gamma \sin \psi + \cos \gamma \sin \theta & \cos \gamma \cos \psi - \sin \gamma \sin \psi \sin \theta & -\cos \psi \sin \theta \\ -\cos \gamma \cos \theta \sin \psi + \sin \gamma \sin \theta & \cos \theta \sin \gamma + \cos \gamma \sin \psi \sin \theta & \cos \gamma \cos \psi \end{pmatrix} \quad (3)$$

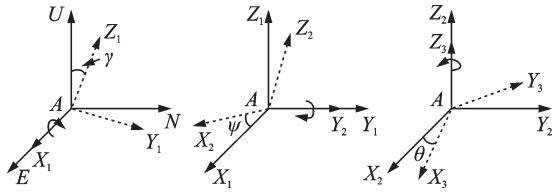


Fig.6 Attitude rotation change

(4) The spatial aiming pointing vector T_2 in the carrier coordinate system can be obtained by Eq.(4). φ_{iu} , φ_{ie} , φ_{im} and φ_u , φ_e , φ_n are the rotation angle of the platform attitude and the LCT installation position relative to the ENU coordinate system and the attitude standard position on the roll, pitch and yaw axis systems, respectively.

$$T_2 = (x, y, z)^T = C_T(\varphi_e, \varphi_n, \varphi_u) C_T(\varphi_{ie}, \varphi_{im}, \varphi_{iu}) C_e^g T_0 \quad (4)$$

(5) Through the above correction, the spatial direction vector of the LCT coordinate system is obtained, and then the vector is converted into the rotation angle of the azimuth axis and the rotation angle of the pitch axis by applying Eq.(5), which is the final spatial angular direction of LCT.

$$\begin{cases} \theta_{Az} = \arctan(x/y) \\ \theta_{El} = \arctan(z/\sqrt{x^2 + y^2}) \end{cases} \quad (5)$$

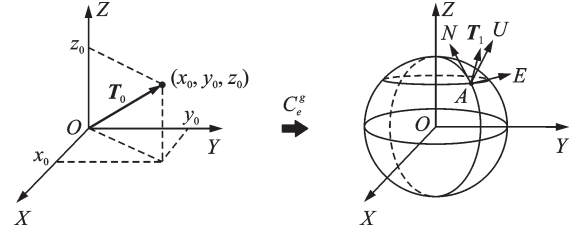


Fig.5 T_1 in ENU coordinate system

the geographic coordinate system, the attitude correction must be performed according to the real-time attitude data of the carrier and the installation error of the terminal. If there is no attitude declination and installation error, the azimuth and pitch axis in the terminal coordinate system are equal to the U axis and N axis respectively, then the attitude compensation rotation matrix is shown in Eq.(3), and the rotation is shown in Fig.6.

2.3 Scanning strategy

The divergence angle of the laser cannot be too large due to the limitation of the optical power. In this experiment, the power of the beacon laser is 1 W, and the divergence angle is 1 mrad. If the beacon optical signal cannot be detected when the LCT starts pointing, it needs to start the scanning strategy. The Archimedes Spiral is chosen as the scanning curve model. In comparison to rectangular scanning or other scanning methods, it is more efficient in covering the uncertainty area from high to low probability. The screw pitch, screw speed, and sweep range are adjusted to create the sweep curve^[23].

The pitch b can be set according to the local beacon divergence angle FOV , where $2\pi b = \eta \cdot r(FOV)$, $\eta \in (0.4-0.8)$, the screw speed v_θ needs to be selected according to the motor control accuracy of the terminal and the feedback frequency of the detector. The scanning effect within the scanning range R is shown in Fig.7.

Archimedes Spiral can be expressed by

$$r = a + b\vartheta \quad (6)$$

where a is the distance between the scanning starting point and the polar origin, and b the value of the

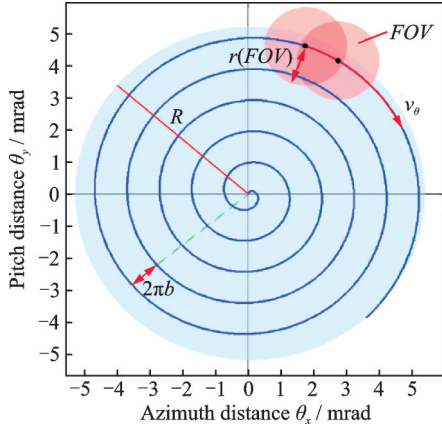


Fig.7 Scanning effect

sweep radius r corresponding to the increase of the helix's unit angle. When scanning begins at the origin, $a=0$.

The polar coordinate representation is shown as

$$\begin{cases} \theta_x = r \cos \vartheta \\ \theta_y = r \sin \vartheta \end{cases} \quad (7)$$

The spiral scanning with identical linear velocity can be obtained by

$$\int_0^{\vartheta} \sqrt{\left(\frac{d\theta_x}{d\vartheta}\right)^2 + \left(\frac{d\theta_y}{d\vartheta}\right)^2} d\vartheta = v_{\theta} \cdot t \quad (8)$$

where t is the unit control time.

Substituting Eqs.(6, 7) into Eq.(8) and evaluating the time derivative yields

$$\dot{\vartheta} = f(t, \vartheta) = v_{\theta} / (b \sqrt{1 + \vartheta^2}) \quad (9)$$

The ideal control system is a continuous model, but it cannot achieve continuous output in practice. Here, we use the method of Runge Kutta to solve the differential Eq.(9), which can improve the approximation accuracy of discrete system. Under the same order, its calculation accuracy is higher than that of the Euler expansion method.

The functional expression of fourth order Runge Kutta is as follows

$$\vartheta_{i+1} = \vartheta_i + h \times (k_1 + 2 \times k_2 + 2 \times k_3 + k_4) / 6 \quad (10)$$

$$\begin{cases} k_1 = f(t_0, \vartheta_0) \\ k_2 = f(t_0 + h/2, \vartheta_0 + h \times k_1/2) \\ k_3 = f(t_0 + h/2, \vartheta_0 + h \times k_2/2) \\ k_4 = f(t_0 + h, \vartheta_0 + h \times k_3) \end{cases} \quad (11)$$

where t_0 is the starting point of the calculation time, i the control cycle count, ϑ_0 the initial scanning angle, h the step length; k_1 , k_2 , k_3 and k_4 are the inter-

mediate quantities of the calculation process. $h=1$ is commonly used in discrete control systems. After the approximate value ϑ_i is obtained, the rotation angle of the two axes can be calculated by Eq.(7).

2.4 Acquisition and tracking strategy

The LCT immediately enters the acquisition mode when detecting the beacon laser of the opposite terminal. There is a deviation angle between the incident direction of the received laser and the normal direction of the antenna at the receiving end. Then the beam spot on the detector will deviate from the center of the detector, as shown in Fig.8.

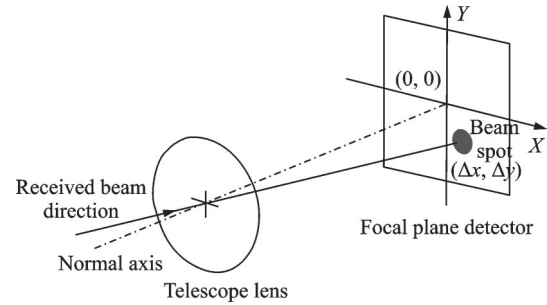


Fig.8 Position of receiving spot in the presence of incidence deviation angle

The offset value coordinates is $(\Delta x, \Delta y)$. According to the output position deviation signal by the detector, the compensation angle of the azimuth pitching axis $(\Delta\theta_{AZ}, \Delta\theta_{El})$ can be obtained by Eq.(12), where f is equivalent focal length of receiving optical path.

$$\begin{cases} \Delta\theta_{AZ} = \arctan(\Delta x/f) \\ \Delta\theta_{El} = \arctan(\Delta y/f) \end{cases} \quad (12)$$

When the beam spot is stable within a certain range of the communication center point, the detector window can be changed to small windows to increase sampling frequency. At the same time, the fast deflection mirror starts working, and the control mode is changed to compound axis tracking mode as a result of the fast deflection mirror and motor's cooperation. Fig.9 depicts the control structure. The system takes the deflection angle of the detector relative to the center as the error feedback link to track the target. After the control proportion conversion (K1), the quantity is transmitted to the fine control unit. The fine control unit starts the

compensation action according to the deviation value of the detector, and transmits the deviation value which deviates from the center value of the dynamic range to the coarse control unit after the low-pass fil-

ter and proportional matching transformation (K2). The coarse pointing compensates the fine tracking action, so as to complete the large dynamic range accurate tracking.

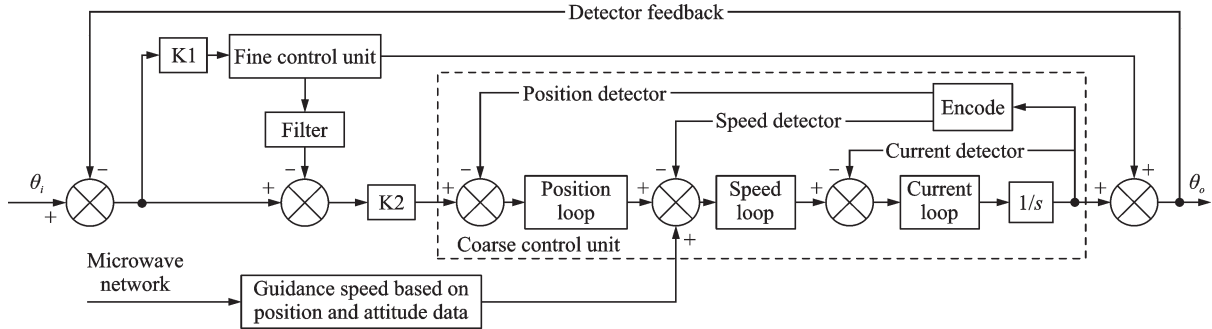


Fig.9 Schematic diagram of tracking control

This experiment uses a single detector, so the coarse and fine control unit use the same detector as the closed-loop feedback. Compound axis tracking has always been a difficulty in laser communication technology^[24]. The microwave network is utilized to convey position and speed data from both sides to each other, and the estimated tracking angle change is incorporated into the speed loop as the open loop's guidance speed input. This architecture can give lead compensator. When the position variation is minor, relative stable speed tracking may be maintained, reducing speed fluctuation and improving tracking accuracy.

3 Experimental Results

3.1 GPS positioning and attitude characteristics of the aerostat platform

We initially tested the repeatability of GPS positioning to better estimate the extent of the pointing uncertainty region. In the experiment, let the aerostat hover at a height of 75 m, restart the system several times and record the GPS positioning data. The measurement results are shown in Fig.10. The variation range of latitude and longitude data is 2—3 m, and the variation range of altitude data is 3—5 m.

The tethered ball has the advantage of long-term small range hovering compared with the aircraft, but at the same time, due to the lack of inter-

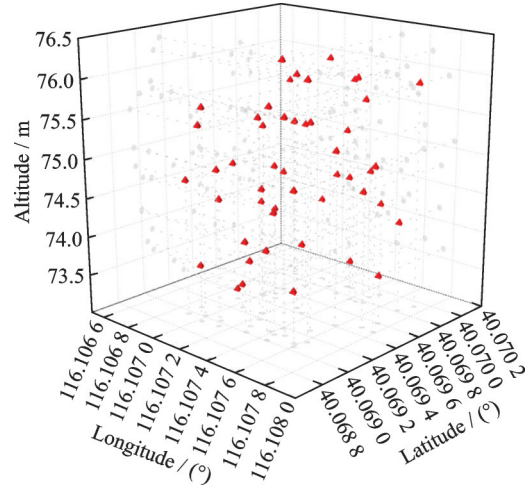


Fig.10 GPS positioning test data

nal attitude maintenance system, its flight attitude will change rapidly with external interference. Fig.11 depicts the platform's attitude change in 16 min at a height of 1 km. The platform's roll and pitch angles change little over time, but the azimuth angle does, with the fastest change speed reaching 4 degrees per.

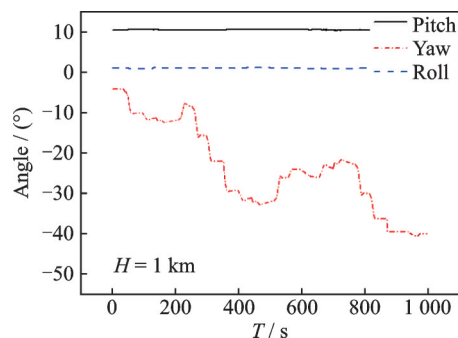


Fig.11 Attitude change at 1 km altitude

As a rapid posture change without compensation can greatly increase the difficulty of scanning capture, the coarse control unit must compensate the posture in real time. Fig.12 depicts the compensation effect for the posture's yaw angle. After posture compensation, the pointing accuracy can be stabilized within 1.2 mrad.

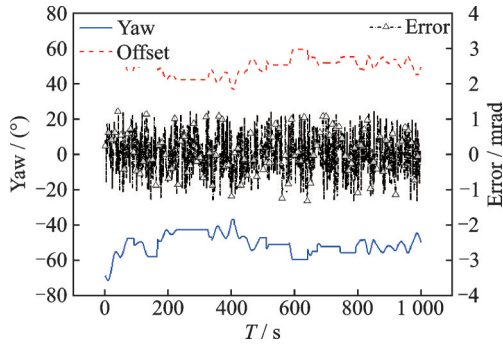


Fig.12 Control compensation effect chart of yaw angle

The attitude data is provided by the platform's inertial navigation device. Since these devices have zero bias and drift, the measurement accuracy decreases as calibration time increases, and this error cannot be avoided. The product data manual states that its attitude drift error is approximately 0.12 (°)/h.

3.2 Platform vibration data

In the open loop scanning capture stage, the vibration error of the platform also has a certain impact on the aiming accuracy. Since the tethered balloon is not powered, its levitation effect is dependent

on the buoyancy of hydrogen or helium in the sphere, the platform cannot generate high-frequency vibration^[25], so we only consider vibration error with the main frequency spectrum concentrated in the 20 Hz range here. The amplitude data after actual measurement is shown in Fig.13. The vibration distribution is approximately the same in three directions, and the standard deviation of the resultant amplitude is about 20 rad.

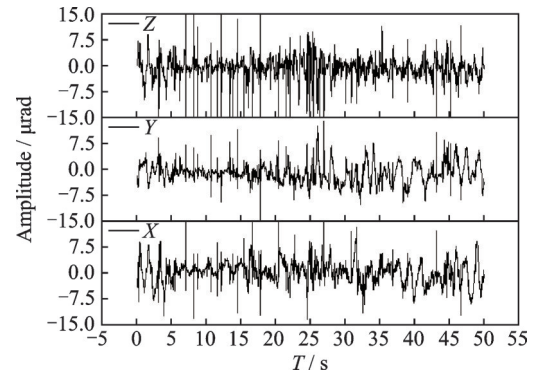


Fig.13 Triaxial vibration amplitude curves

3.3 Scanning and tracking test data

The uncertain field of pointing is based not only on the above measured data, but also on some less influential factors, such as turntable pointing accuracy, angle error caused by shafting thermal stress, and so on. Table 2 provides a detailed breakdown of the overall estimated values. We set the scanning range (R) to 1.5 times the uncertain field

Table 2 Scan range index

Item	Expression	Index	Note
GPS positioning error	σ_1	≤ 0.33 mrad	The link distance is 20 km, the height error is 3—5 m, and the horizontal error is 2—3 m, $\sigma_1 = \sqrt{5^2 + 3^2 + 3^2} \approx 6.557$ m
Compensation error of attitude	σ_2	1.2 mrad	The motor compensates according to the attitude feedback of the gyroscope, but there is a large control deviation due to the low update frequency of the gyroscope attitude data
Attitude drift error	σ_3	1 mrad	The running time of gyroscope after starting and calibration is tentatively 0.5 h, $\sigma_3 \approx 1$ mrad
Pointing error caused by platform vibration	σ_4	20 μ rad	Pointing error caused by platform vibration in open loop aiming
Pointing accuracy error of turntable	σ_5	40 μ rad	Pointing error in the process of movement due to the motor control
Angle error caused by shafting thermal stress	σ_6	20 μ rad	The change of the suspension height and the temperature of the external environment will produce thermal stress on the shafting
Uncertain field of pointing	S	4.8 mrad	$S = 3\sqrt{\sigma_1^2 + \sigma_2^2 + \sigma_3^2 + \sigma_4^2 + \sigma_5^2 + \sigma_6^2}$
Scanning range	R	7.2 mrad	The scanning range is determined by an uncertain field, which ensures that the beacon laser covers the link terminal

of pointing (S), which provides the maximum probability to capture beacon laser in a single scan. The scanning interval is 0.8 mrad, the scanning speed is 0.5 ($^{\circ}$)/s, and the scanning time for the entire area is approximately 23 s.

The scanning position of the beacon laser is recorded by the LCT during several flight tests, as shown in Fig.14. The experiment demonstrates that error estimation can effectively estimate the target's actual spatial position coordinates, ensuring the rapid establishment of the laser communication link.

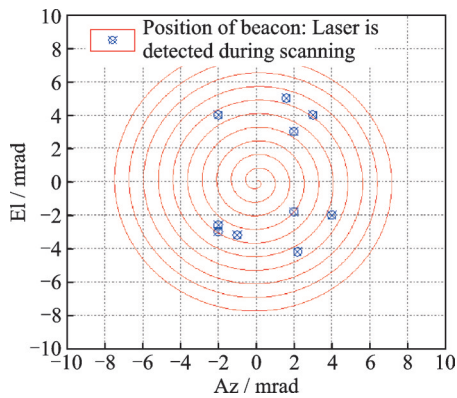


Fig.14 Scanning data

In the tracking state, the fine control unit has an obvious compensation effect on the control residual of the coarse control unit and platform vibration, and can compress the vibration to less than 10% of the original amplitude. Fig.15 depicts the tracking error on the CCD's X and Y axes, and the final synthesis control accuracy is less than 5 μ rad, which meets the needs of laser communication.

3.4 Communication performance verification

After the stable laser link is established, the

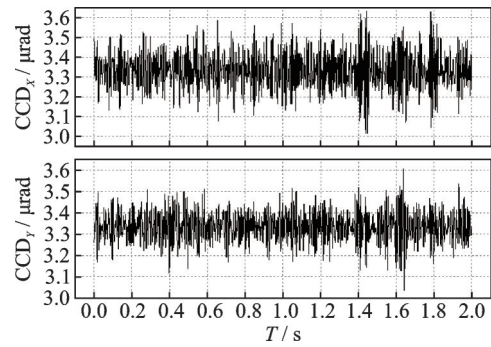


Fig.15 Tracking error

communication function module is opened. The aerostat platform is equipped with the LCT to emit modulated signal light. The ground photos taken by the infrared high-definition camera are transmitted to the receiving terminal through the laser link. The receiving LCT on the ground decodes them and completes the image reconstruction. The data transmission and distribution process are shown in Fig.16.

The resolution of high-definition image is $1\ 920 \times 1\ 600$ pixels, in which gray value of each pixel is 256, and the frame rate is 24 frame/s. The image data captured by the infrared high-definition camera is copied into 48 copies, and then transmitted to the ground monitoring station through the space laser relay link. The integrity of each image is observed through the multi-channel data display of the ground monitoring station, so as to verify its high-speed communication performance. The experimental results show that the image data displayed by multi-channel data is complete, the bit error rate is less than 10^{-6} , and the communication rate of single laser relay link is up to 2.5 Gbit/s.

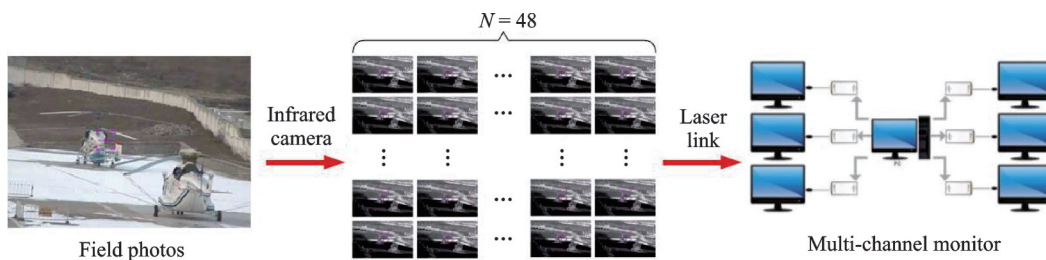


Fig.16 Effect picture of real-time image transmission by infrared camera

4 Conclusions

This paper presents a laser communication re-

lay system based on tethered sphere platforms. An air to ground laser link is established at an altitude of 1 km, the communication rate reaches 2.5 Gbit/s,

which can transmit the real-time image data, captured by the high-definition infrared camera, to the ground monitoring station through the laser carrier. Laser communication distance can be up to 20 km. We introduce the pointing strategy established by the laser communication link in detail, and uses Runge Kutta algorithm to make Archimedean Spiral scan strategy more effective on the discrete system. At the same time, it shows the control mechanism diagram of the tracking system, which uses the low-speed microwave network to provide reliable position and speed guidance for the tracking loop, and improves the tracking performance of the outer loop of the composite tracking system. As a proof of concept demonstration, this experiment has verified the feasibility of the LCT as a high-speed relay node.

In subsequent experiments, we will add detection equipments to detect the BER performance at different transmit powers, and try to verify the communication performance under strong turbulence conditions. A comprehensive evaluation of system communication stability under various working conditions will be completed.

References

- [1] YUAN Yifei. LTE-advanced relay technology and standardization, signals and communication technology[M]. [S.l.]: Springer Publishing Company, 2013.
- [2] SONG K, JI B, HUANG Y, et al. Performance analysis of antenna selection in two-way relay networks[J]. IEEE Transactions on Signal Processing, 2015, 63(10): 2520-2532.
- [3] CHEN S Z, KANG S L. A tutorial on 5G and the progress in china[J]. Frontiers of Information Technology & Electronic Engineering, 2018, 19(3): 6-19.
- [4] TOYOSHIMA M, LEEB W R. Comparison of microwave and light wave communication systems in space applications[J]. Optical Engineering, 2005, 46(1): 015003.
- [5] JIANG Huilin, TONG Shoufeng, ZHANG Lizhong. The technologies and systems of space laser communication[M]. Beijing: National Defense Industry Press, 2010. (in Chinese)
- [6] YANG Jian, BAO Fangdi, YU Siyuan. Ground-air-space cooperative laser communication technology and application[M]. Beijing: China Science Publishing & Media Ltd. 2022. (in Chinese)
- [7] MA Jing, TAN Liying, YU Siyuan. Satellite optical communication[M]. [S.l.]: National Defense Industry Press, 2015. (in Chinese)
- [8] KONISHI M, NISHIMAKI T, SHIBATA Y, et al. A study of co-channel spectrum-sharing system between HAPS and terrestrial mobile communication networks[C]//Proceedings of 2020 IEEE the 91st Vehicular Technology Conference (VTC2020-Spring). [S.l.]: IEEE, 2020.
- [9] ZHANG H, YANG Z, YANG L, et al. Power control for 5G user-centric network: Performance analysis and design insight[J]. IEEE Access, 2017, 4: 7347-7355.
- [10] ALZENAD M, SHAKIR M Z, YANIKOMEROG-LU H, et al. FSO-based vertical backhaul/fronthaul framework for 5G+ wireless networks[J]. IEEE Communications Magazine, 2018, 56(1): 218-224.
- [11] XU Wei, ZHAO Rui, YANG Yulin. Throughput analysis of energy harvesting relay selection systems with direct link[J]. Signal Processing, 2019, 35(3): 472-480.
- [12] VALLESTERO N J, PRASAD N S, CARRANO J C, et al. Free-space optical communication systems (FOCUS): A U.S. army overview[J]. Applied Optics, 2002, 44(13): 2530-2540.
- [13] BUCHTER K D. Modeling of high-capacity aeronautical communication networks with free-space optical links[C]//Proceedings of 2015 the 4th International Workshop on Optical Wireless Communications (IWOW). [S.l.]: IEEE, 2015.
- [14] BÖHMER K, GREGORY M, HEINE F, et al. Laser communication terminals for the European data relay system[C]//Proceedings of Free-Space Laser Communication Technologies XXIV. Bellingham: SPIE, 2012, 8246: 79-85.
- [15] ABOU-RJEILY C, KADDOUM G, KARAGI-ANNIDIS G K. Ground-to-air FSO communications: When high data rate communication meets efficient energy harvesting with simple designs[J]. Optics Express, 2019, 27(23): 34079.
- [16] MUKHERJEE B. WDM optical communication networks: Progress and challenges[J]. IEEE Journal on Selected Areas in Communications, 2000, 18(10): 1810-1824.
- [17] TOPCU O, HENNIGER H, GROBE L, et al. Lightweight, mobile free-space optical communications in disaster scenarios for transmission of Earth observation data: Feasibility study[C]//Proceedings of

- Free-Space & Atmospheric Laser Communications XI. [S.l.]: SPIE, 2011, 8162: 17-29.
- [18] HAAN H, SIEMENS C. Airborne optical communication terminal: First successful link from Tenerife to the GEO Alphasat[J]. Proceedings of SPIE, 2019, 11133: 1113306.
- [19] WU R, ZHAO X, LIU Y, et al. Initial pointing technology of line of sight and its experimental testing in dynamic laser communication system[J]. IEEE Photonics Journal, 2019, 11(2): 1-8.
- [20] CHY A, BSG A, YJC A, et al. Bidirectional free space optical communication (FSO) in WDM access network with 1000-m supportable free space link- ScienceDirect[J]. Optics Communications, 2019, 435: 394-398.
- [21] WEN Chuanhua, LI Yuquan. The optical system in the laser space communication[J]. Optical Communication Technology, 2003, 27(7): 24-27.
- [22] MICHAEL P, YOSEF R, GARY P, et al. Spacecraft attitude and orbit control[M]. New York: Princeton Satellite Systems Inc., 2012.
- [23] SCHEINFELD M, KOPEIKA N S, MELAMED R. Acquisition system for microsatellites laser communication in space[J]. Proceedings of SPIE—The International Society for Optical Engineering, 2000. DOI: 10.1117/12.384308.
- [24] ZHANG Min, TONG Shoufeng. Research on single-sensor and multiple-axis tracking control system for spatial laser communication[J]. Laser and Infrared, 2019, 49(8): 983-986.
- [25] RAJANI A, PANT R S, SUDHAKAR K. Dynamic

stability analysis of a tethered aerostat[J]. Journal of Aircraft, 2010, 47(5): 1531-1538.

Acknowledgement This work was supported by the National Natural Science Foundation of China (No.91838302).

Authors Prof. YU Siyuan received the Ph.D. degree in physics and electronics from Harbin Institute of Technology in 2002. At present, he is a professor and doctoral supervisor of Harbin Institute of Technology; Director of Heilongjiang Key Laboratory of laser space communication technology and application. In 1996, he began to engage in the research of satellite optical communication.

Dr. LI Bo received M. S. degree in electronic science and technology in 2015 from Harbin Institute of Technology, where he is currently working toward the Ph.D. degree in electronic science and technology. His research interests include the overall technology of space optical communication, beam aiming, acquisition and tracking control technology, optical signal atmospheric transmission compensation technology and so on.

Author contributions Prof. YU Siyuan and Dr. LI Bo designed the study, compiled the models, conducted the analysis, interpreted the results and wrote the manuscript. Prof. CAO Kairui proposed the system's control model and assessed the communication performance. Dr. DU Hairui and Dr. HAO Guanglu contributed to the discussion and background of the study. All authors commented on the manuscript draft and approved the submission.

Competing interests The authors declare no competing interests.

(Production Editor: WANG Jing)

系留球和地面之间的自由空间光通信中继系统设计与验证

于思源, 李 博, 曹开锐, 郝广路, 杜海瑞

(哈尔滨工业大学可调谐激光技术国家级重点实验室, 哈尔滨 150001, 中国)

摘要: 目前微波移动中继网络存在中继距离短、数据传输速率慢、功耗高、工作频率受限等问题。本文使用激光通信技术构建了一个中继系统, 该系统实现了系留球和地面基站之间红外高清图像数据的实时转发, 通信距离超过 20 km。实验的成功为激光通信技术作为机载通信中继站的应用提供了技术参考。针对初始瞄准指向角度不可预测、平台姿态快速变化等特殊场景, 提出了一种用于确定扫描角域的评估方法和姿态稳定性补偿的方案来解决这些问题。通过 4 阶 Runge-Kutta 迭代方法规避复杂的微积分计算, 提高了扫描算法的精度。将基于目标空间位置和自身姿态变化的数据通过前馈补偿算法引入到闭环跟踪系统的速度环中, 有效提高了系统的跟踪稳定性。未来将实现空对空的激光链路中继网络实验。

关键词: 空间光通信; 激光链路; 瞄准、捕获和跟踪